Solid State Sciences 43 (2015) 9–14

Contents lists available at ScienceDirect

Solid State Sciences

journal homepage: www.elsevier.com/locate/ssscie

Theoretical study of the structural, elastic, electronic and optical properties of $XCaF_3$ (X = K and Rb)

B. Ghebouli [a], M. Fatmi [b], M.A. Ghebouli [b, c, *], H. Choutri [c], L. Louail [b], T. Chihi [b], A. Bouhemadou [d], S. Bin-Omran [e]

[a] Laboratory of Studies of Surfaces and Interfaces of Solids Materials, University of Ferhat Abbas, Setif 01, 19000, Algeria
[b] Research Unit on Emerging Materials (RUEM), University of Ferhat Abbas, Setif 01, 19000, Algeria
[c] Microelectronic Laboratory (LMSE), University of Bachir Ibrahimi, Bordj-Bou-Arreridj, 34000, Algeria
[d] Laboratory for Developing New Materials and their Characterizations, University of Ferhat Abbas, Setif 01, 19000, Algeria
[e] Department of Physics and Astronomy, College of Science, King Saud University, P.O. Box 2455, Riyadh 11451, Saudi Arabia

ARTICLE INFO

Article history:
Received 24 December 2014
Received in revised form
9 March 2015
Accepted 10 March 2015
Available online 12 March 2015

Keywords:
The alkaline earth fluorides
Elastic properties
Ab initio calculations

ABSTRACT

The PLANE WAVE pseudo-potential method within density functional theory (DFT) has been used to investigate the structural, elastic, electronic and optical properties of $XCaF_3$ (X = K and Rb) insulating. The studied compounds show a weak resistance to shear deformation compared to the resistance to the unidirectional compression. $KCaF_3$ and $RbCaF_3$ are considered ductile. The elastic constants and related parameters were predicted. The stiffness is more important in $KCaF_3$, whereas, the lateral expansion is more important in $RbCaF_3$. $KCaF_3$ and $RbCaF_3$ have R- Γ indirect band gap. The main peaks in the imaginary part of the dielectric function correspond to the transition from the occupied state F_p to the unoccupied states Ca: s or K, Rb: p. At lower energies, $KCaF_3$ and $RbCaF_3$ show the same optical properties. Under pressure effect, the peaks of imaginary part of dielectric function were shifted toward high energy.

1. Introduction

The alkaline earth fluorides are wide band gap, exhibit fast ion conduction up to their melting points [1], are prospective candidates for vacuum-ultraviolet-transparent lenses used in optical lithography steppers [2] and are also promising for fast scintillators [3]. The preparation of perovskites $XCaF_3$ (X = K and Rb) followed the procedure described in the literature [4]. XF and CaF_2 were first mixed and ground in a molar ratio of 1:1. The obtained powder was pressed into a pellet, closed in a gold tube, and then sealed in a silica tube under argon. The silica tube was annealed, followed by a slow cooling of the ampoule. The $KCaF_3$ and $RbCaF_3$ have been synthesized [1,5] and were found to have cubic symmetry of perovskite structure [6]. This family of perovskites fluorides, $XCaF_3$ shows a larger X–F distance than the Ca–F one. The study of ionic conductivity in $KCaF_3$ by molecular dynamics (MD) simulations has been carried out with both defect free and defect containing models [7,8]. The Ca ion in $XCaF_3$ perovskites plays an important role in transport [6]. The optical properties of this type of perovskites are anisotropic, show the phenomenon of birefringence and their geometry is related to the chemical composition, temperature and pressure [9]. The structural, elastic, thermodynamic and optical properties of these compounds were investigated experimentally [2]. The use of first principles calculations offers one of the most powerful tools for carrying out theoretical studies of an important number of physical and chemical properties of the condensed matter with great accuracy [10,11]. In the present work, we applied a detailed theoretical study of the structural, elastic, electronic and optical properties of the family $XCaF_3$ (X = K and Rb) using the density functional theory (DFT).

From the perspective of materials science, the elastic constants contain some of the more important information which can be obtained from ground state total energy calculations. The elastic constants are related to some fundamental properties such as interatomic potential, equation of state, phonon spectra, specific heat, Debye temperature and melting point. The elastic constants play an important role in determining the strength of the material. The elastic constants of the $XCaF_3$ (X = K and Rb) perovskite

* Corresponding author. Microelectronic Laboratory (LMSE), University of Bachir Ibrahimi, Bordj-Bou-Arreridj, 34000, Algeria.
E-mail address: med.amineghebouli@yahoo.fr (M.A. Ghebouli).

http://dx.doi.org/10.1016/j.solidstatesciences.2015.03.009

fluorides have been not yet measured either calculated. So the calculation of the elastic constants of these materials is one of the main objectives of the present work.

The paper is organized as follows: in Section 2, we briefly described the computational techniques used in this work. Results and discussions of our study will be presented in Section 3. Finally, conclusions are given in Section 4.

2. Computational method

The first-principles calculations were performed using the CASTEP code [12], which is an implementation of the plane-wave pseudo-potential total energy method based on the density functional theory (DFT). The interactions of electrons with ion cores were represented by the Vanderbilt-type ultrasoft pseudo-potentials [13] and norm-conserving pseudo-potentials for K, Rb, Ca and F atoms. The exchange-correlation potential was treated within the generalized gradient approximation (GGA) of Perdew, Burke and Ernzerhof [14]. The plane-wave basis set cut-off was 350 eV for all cases. The special points sampling integration over the Brillouin zone was employed by using the Monkhorst–Pack method with $8 \times 8 \times 8$ special k-point mesh [15]. These parameters were sufficient in leading to well converged total energy, geometrical configuration and elastic moduli. The Broyden-Fletcher-Goldfarb-Shanno (BFGS) minimization technique [16], which provides a fast way of finding the lowest energy structure, was used in the geometry optimization. The self-consistant calculation for the geometry optimization were considered to be converged when the difference in total energy is within 5×10^{-6} eV/atom, maximum ionic Hellmann-Feynman force is within 0.01 eVÅ^{-1} and maximum stress is within 0.02 eVÅ^{-3}.

3. Results and discussions

3.1. Crystal structure

The cubic unit cell of $XCaF_3$ (X = K and Rb) contains one molecule with the X sitting 1b at (0.5, 0.5, 0.5), the Ca 1a at (0, 0, 0) and F 3d at (0.5, 0, 0). The calculated lattice constant, bulk modulus and its pressure derivative at equilibrium determined by fitting the total energy versus the volume to the Murnaghan equation of state [17] are summarized in Table 1. Also shown for comparison are the experimental (theoretical) values of 4.41 Å and 4.455 Å [18,19] (4.424 Å and 4.452 Å [2]) for $KCaF_3$ and $RbCaF_3$.

Our calculated bulk modulus and its pressure derivative are in reasonable agreement with the theoretical ones (49 GPa and 4.038) and (49.77 GPa and 5) [2]. The bulk modulus is a measure of the crystal rigidity, thus a lower compressibility is for small crystal rigidity.

3.2. Elastic properties

The determination of the elastic constants requires the knowledge of the curvature of the energy curves as a function of strain for selected deformation of the unit cell. The strains are considered with and without volume conservation. We considered small lattice distortions in order to remain within the elastic domain of the crystal. The predicted PBE-GGA elastic constants and bulk modulus at zero pressure for $KCaF_3$ and $RbCaF_3$ are listed in Table 1. To date, no experimental or theoretical data for the elastic stiffness are available in the literature to be compared with our theoretical results. Then, our results can provide reference data for future investigations. The C_{44}, which reflects the resistance to shear deformation, is about 10.7% (13.7%) lower than C_{11} for $KCaF_3$ ($RbCaF_3$), which is related to the unidirectional compression along the principal crystallographic directions, indicating the weak resistance to shear deformation compared to the resistance to the unidirectional compression. The stability of a cubic crystal under pressure effect requires the verification of the following criteria [20]:

$$\{(C_{11} + 2C_{12} + P) > 0, (C_{44} - P) > 0, (C_{11} - C_{12} - 2P) > 0\} \quad (1)$$

The calculated elastic constants satisfy the above criteria over the pressure range, suggesting the mechanical stability of $KCaF_3$ and $RbCaF_3$. The effect of pressure on elastic constants and bulk modulus is shown in Fig. 1. All these parameters increase with increasing pressure, except the decrease on C_{44} is weaker. The elastic parameters of $KCaF_3$ and $RbCaF_3$ such as shear and Young moduli, Poisson's coefficient B/G ratio are reported in Table 1. The shear modulus G represents the resistance to plastic deformation, while the bulk modulus B represents the resistance to fracture. A high B/G ratio is associated with ductility, whereas a low value corresponds to brittle nature. The calculated B/G value of $KCaF_3$ and $RbCaF_3$ classifies these materials as ductile and can support large thermal shocks. In Table 1, we listed our results for the pressure derivatives $\partial C_{11}/\partial p$, $\partial C_{12}/\partial p$, $\partial C_{44}/\partial p$. We can notice that C_{11} is more sensitive to the pressure than C_{12} and C_{44}. The atoms are closer under high pressure, then the electrostatic repulsive force among the electrons and the covalence increases. So it is difficult for the atoms to move due to the saturation of the covalence. Young's modulus is a measure of the stiffness of a given material, while Poisson's ratio is the ratio of the contraction or transverse strain to the extension or axial strain, when a sample is stretched. We note that Young modulus decreases from $KCaF_3$ to $RbCaF_3$. This implies that the stiffness of $KCaF_3$ is more important than that of $RbCaF_3$. The values of σ obtained for material of interest are ranging between −1 and 0.5. However, one should observe that σ decreases from $KCaF_3$ to $RbCaF_3$, thus under a given compression, the lateral expansion is more important in $RbCaF_3$. The calculated density ρ, longitudinal, transverse and average sound velocity v_l, v_t and v_m and

Table 1
Calculated lattice constant a_0 (Å), bulk modulus B_0 (GPa) and its pressure derivative B', the pressure derivatives of elastic constants, shear and Young moduli, Poisson's coefficient and B/G ratio for $KCaF_3$ and $RbCaF_3$ perovskites.

	a_0 (Å)	B_0 (GPa)	B_0'	C_{11}	C_{12}	C_{44}	B	$\frac{\partial C_{11}}{\partial P}$	$\frac{\partial C_{12}}{\partial P}$	$\frac{\partial C_{44}}{\partial P}$	$\frac{\partial B}{\partial P}$	G	E	σ	B/G
$KCaF_3$															
T. W.	4.3236	61.9	4.295	143.9	19.2	15.8	60.8	8.491	1.676	−0.24	4.128	28.5	73.9	0.297	2.134
Exp.	4.41 [18]														
Other	4.424 [2]	49 [2]	4.038												
$RbCaF_3$															
T. W.	4.3525	63.9	4.124 [2]	139.3	23.2	19.2	61.9	8.209	1.883	−0.01	3.992	30.4	78.5	0.288	2.031
Exp.	4.455 [19]														
Other	4.452 [2]	49.7 [2]	5 [2]												

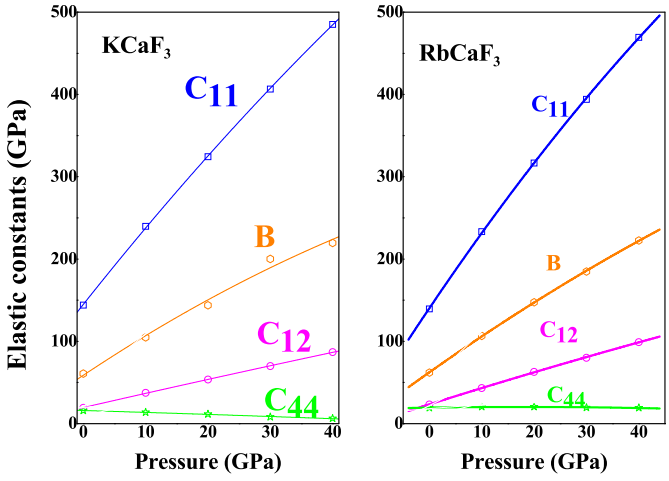

Fig. 1. The effect of pressure on elastic moduli.

Debye temperature θ_D for the $KCaF_3$ and $RbCaF_3$ perovskites are listed in Table 2. $RbCaF_3$ show the lower velocities and Debye temperature. The calculated elastic wave velocities of $KCaF_3$ and $RbCaF_3$ perovskites along [100], [110] and [111] directions are listed in Table 3. Longitudinal waves (shear waves) are fastest (slowest) along [100].

A useful visualization of the elastic anisotropy can be obtained by plotting a three-dimensional representation (3D) of the dependence of Young's modulus E on direction in a crystal. For cubic structure, the directional dependence of Young's modulus in 3D representations can be given by [21]:

$$E(\vec{n}) = 1\Big/\left[S_{11} - (2S_{11} - 2S_{12} - S_{44})\left(n_1^2n_2^2 + n_1^2n_3^2 + n_2^2n_3^2\right)\right] \quad (2)$$

where S_{ij} are elastic compliance constants, and n_1, n_2 and n_3 are the directional cosines to the x-, y- and z-axes, respectively. Eq. 2 determines a 3D closed surface, and the distance from the origin of the system coordinates to this surface is equal to young's modulus in a given direction. For a perfectly isotropic material this surface would be a sphere, but often this is not the case even for cubic crystals. The obtained 3D directional dependence of Young's moduli for $KCaF_3$ and $RbCaF_3$ are shown in Fig. 2. Clearly, Fig. 2 shows obvious deviations from spherical shape for the two considered compounds.

To further reveal the anisotropic features in more detail, 2D projection of the 3D directional dependence of Young's modulus is depicted also in Fig. 2. Fig. 2 shows that on the *ab*-plane, the Young's modulus has a maximum value along the crystallographic axes *a*, *b* and *c*, whereas it has a minimum along the bisector direction in each of the *ab*-, *bc*- and *ac*-coordinate plane.

3.3. Electronic properties

We illustrated in Fig. 3 the band structures of $KCaF_3$ and $RbCaF_3$ compounds along the high-symmetry X, R, M and Γ in the first Brillouin zone for the optimized lattice constants. The computed band structures show that these compounds are insulating with Γ−R indirect band gap. We show in Fig. 4 the plots of the pressure variation of the direct and indirect gaps. The fundamental gap increases monotonously with increasing pressure, and it changes from Γ−R to Γ−Γ at about 6 GPa. We obtained the gap at zero pressure $E_g(0)$, the first and second order pressure derivatives α and β of the direct and indirect gaps (Γ−Γ), (R−R), (X−X), (M−M) and (Γ−R) by fitting our energy gaps data using a least squares procedure:

$$E_g(P) = E_g(0) + \alpha P + \beta P^2 \quad (3)$$

The results are given in Table 4 for both $KCaF_3$ and $RbCaF_3$ compounds using GGA.

We have also calculated the total and atomic site projected densities of states (TDOS and PDOS) of these compounds as shown in Fig. 5, within the energy interval from (E_F − 3 eV) up to (E_F +15 eV). The upper valence bands situated in the range (−3 eV to E_F) for both $KCaF_3$ and $RbCaF_3$ is principally due to the F: p site. The conduction bands are mainly (K and Rb: s and p) for both $KCaF_3$ and $RbCaF_3$ respectively. The fundamental band gap at equilibrium corresponds to the electronic transition between (F:p) site to (K:s and Rb:s) states.

The effective charge-carrier mass is one of the main factors that determine the transport properties and electrical conductivity of a material. Generally speaking, the smaller the effective masses of the carriers are, the faster the photogenerated carriers are. Consequently, a light effective mass can promote the migration of carriers and suppress the recombination of carriers. Here, the effective charge-carrier mass m* was evaluated by fitting the $E - k$ diagram near the valence-band maximum (VBMa) and conduction-band minimum (CBMi) with a paraboloid; the effective mass m^* (in unit of m_0, where m_0 denotes the electron rest mass) at a given point along the direction given by $\vec{k}$ is:

$$\frac{1}{m^*} = \frac{m_0}{\hbar^2}\frac{\partial^2 E(k)}{\partial^2 k} \quad (4)$$

The evaluated effective charge-carrier masses from the band dispersions of the valence band maximum and conduction band minimum wards in the Brillouin zone are summarized in Table 5 for two considered materials. The effective electron mass is indicated by the under script "*e*" (m_e^*) and the hole mass by "*h*" (m_h^*). From Table 5 we can note: (i) the electronic states at the conduction-band minimum are much more dispersive than the topmost valence band states, consequently, effective masses of the conduction band electrons are lighter than those of the valence band holes and hence the influence of the later on the electrical conductivity will be minimal, (ii) the effective masses of electrons in the considered materials for the $\Gamma \rightarrow R$ and $\Gamma \rightarrow M$ directions in the BZ are practically equal, hence, the conduction band electron mobility and electrical

Table 2
Calculated density ρ (g/cm^3), longitudinal, transverse and average sound velocity v_l, v_t and v_m (m/s) and Debye temperature θ_D (K) for the $KCaF_3$ and $RbCaF_3$ perovskites.

	ρ	v_l	v_t	v_m	θ_D
$KCaF_3$	**2.7986**	**5943**	**3191**	**3564**	**489**
$RbCaF_3$	**3.6759**	**5283**	**2879**	**3212**	**482**

Table 3
Elastic wave velocities (m/s) within *GGA* for different propagation directions for $KCaF_3$ and $RbCaF_3$ perovskites.

	[100]			[110]			[111]		
	v_L	v_{T1}	v_{T2}	v_L	v_{T1}	v_{T2}	v_L	v_{T1}	v_{T2}
$KCaF_3$	7170	2376	2376	5897	6675	2376	5407	4090	4090
$RbCaF_3$	6155	2285	2285	5227	5619	2285	4878	3502	3502

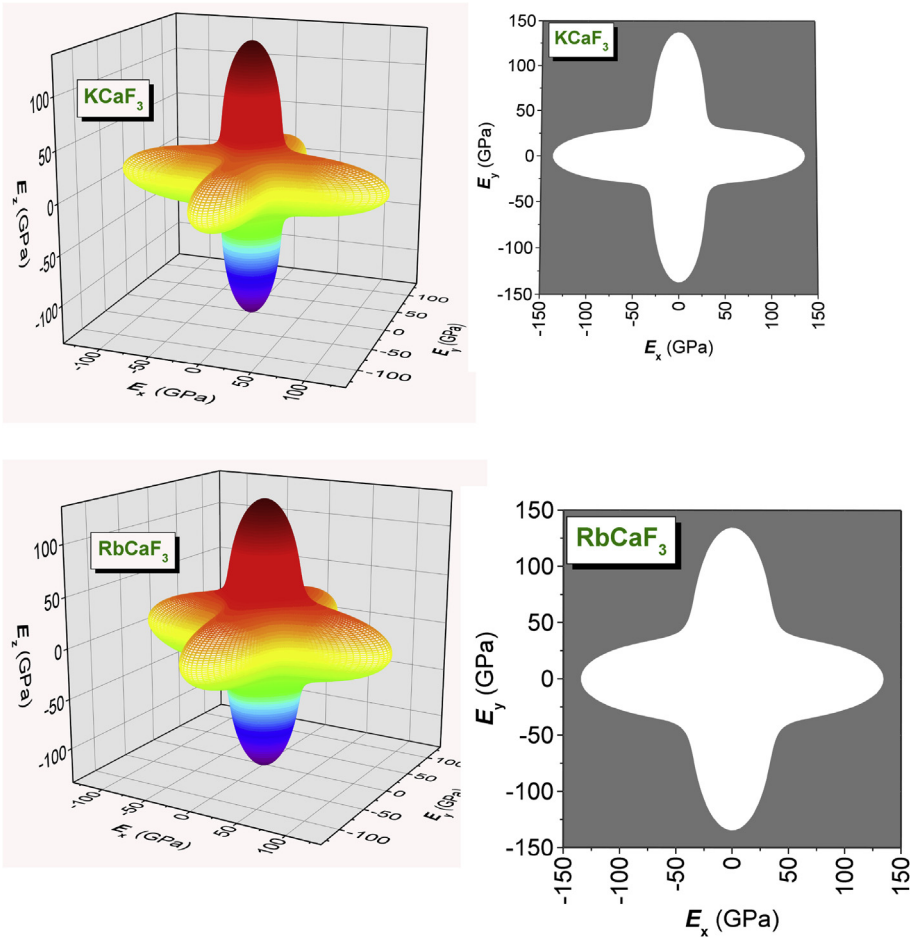

Fig. 2. 3D and 2D (in the *ab*-plane) directional dependence of the Young's modulus for $KCaF_3$ and $RbCaF_3$.

conductivity of the herein studied materials are expected to be isotropic, (iii) the valence-band maximum the $R \rightarrow M$ direction is flat, representing the rather large hole effective n this direction (iv) the dependence of the effective masses of holes on the crystallographic direction demonstrates the anisotropy of this property, hence, the valence band hole conductivity are expected to be anisotropic as well.

3.4. Optical properties

We display the real ε_1 and imaginary ε_2 parts of the dielectric function at zero pressure as a function of photon energy in Fig. 6.

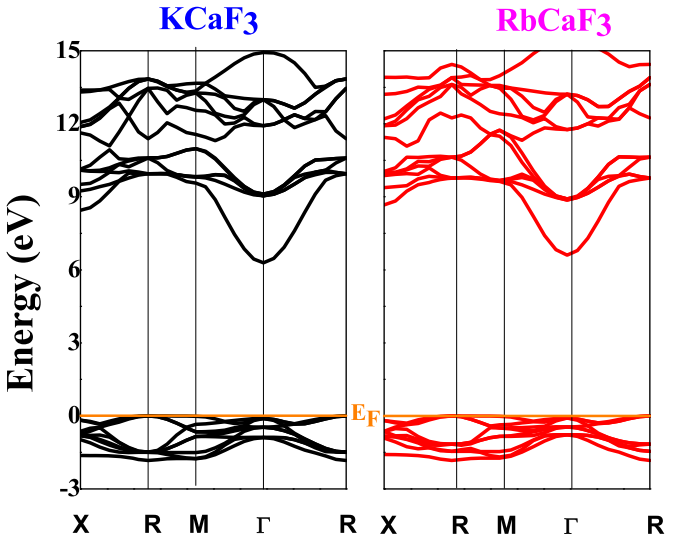

Fig. 3. The band structures of $KCaF_3$ to $RbCaF_3$ compounds along the high-symmetry X, R, M and Γ in the first Brillouin zone.

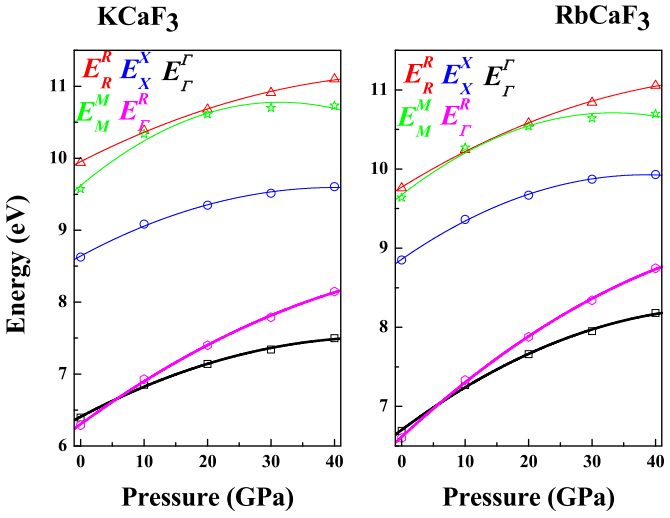

Fig. 4. The plots of the pressure variation of the direct and indirect gaps.

Table 4
The gap at zero pressure $E_g(0)$, the first and second order pressure derivatives α and β of the direct and indirect gaps for $KCaF_3$ and $RbCaF_3$ perovskites.

	$E_{\Gamma-\Gamma}$	E_{R-R}	E_{X-X}	E_{M-M}	$E_{\Gamma-R}$
$KCaF_3$					
$E_g(0)$ (eV)	6.69	9.76	9.64	8.85	6.6
α (eV/Pa)	0.059	0.049	0.062	0.055	0.074
β (10^{-4}) (eV/GPa^{-1})	−5.73	−4.35	−9.37	−7.23	−5.28
$KCaF_3$					
$E_g(0)$ (eV)	6.39	9.94	9.57	8.62	6.29
α (eV/Pa)	0.046	0.044	0.074	0.047	0.064
β (10^{-4}) (eV/GPa^{-1})	−4.91	−4.13	−11.8	−5.91	−4.58

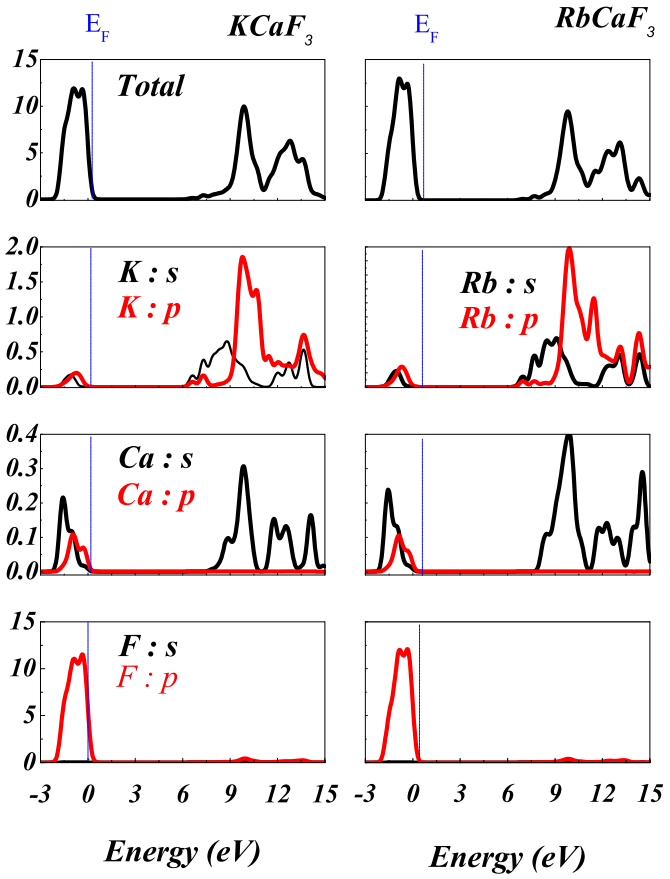

Fig. 5. The total and atomic site projected densities of states (TDOS and PDOS).

Table 5
Calculated effective masses of the electrons m_e^* and holes m_{hh}^* (in units of free electron mass m_0) for the $KCaF_3$ and $RbCaF_3$ compounds.

System	m_e^*		m_h^*	
	$\Gamma - M$	$\Gamma - R$	$R - M$	$R - X$
KCaF3	0.036	0.036	4.716	0.391
RbCaF3	0.031	0.031	3.228	0.393

The identification of interband transitions responsible for the structure of ε_2 requires the use of the band structure. The threshold energy of the dielectric function occurs at 5.4 and 5.7 eV for $KCaF_3$ and $RbCaF_3$. The main peaks in the spectra are located at $E_1 = 10.18$ (10.07) eV and $E_2 = 12.8$ (12.6) eV for $KCaF_3$ ($RbCaF_3$), which correspond to the transition from the occupied state F_p (valence band) to the unoccupied states Ca: s or K, Rb: p (conduction band).

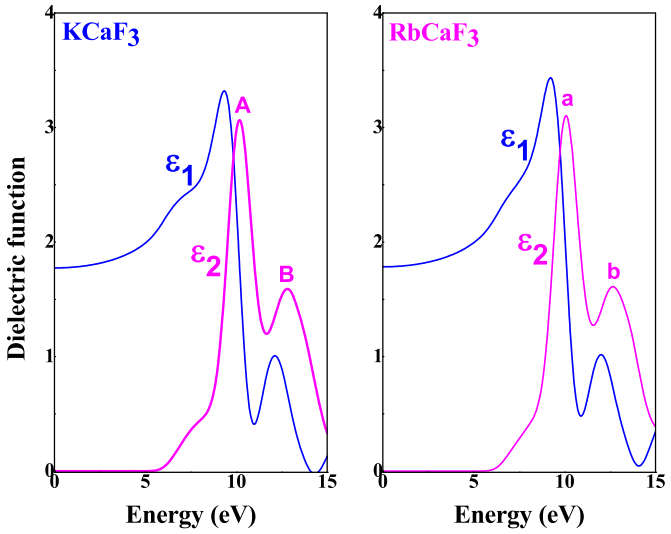

Fig. 6. The real ε_1 and imaginary ε_2 parts of the dielectric function at zero pressure as a function of photon energy.

The first peak coincides with the R–R transition. The static dielectric constant $\varepsilon_1(0)$ is 1.77 for $KCaF_3$ and $RbCaF_3$ respectively. The imaginary part as a function of photon energy for P = 0 and P = 40 GPa is shown in Fig. 7. Under pressure effect, all peaks were shifted toward high energy. The computed linear absorption, reflectivity and loss function are displayed in Fig. 8. The absorption started at about 6 eV. The maximum of reflectivity is 0.18 (0.16) at 15.54 eV (14.09 eV). The maximum of loss is 1.74 and 2.63 at 15 eV and 14.66 eV for $KCaF_3$ and $RbCaF_3$. At lower energies, the absorption, reflectivity and loss are practically the same both $KCaF_3$ and $RbCaF_3$ compounds.

4. Conclusion

The perovskites $KCaF_3$ and $RbCaF_3$ were studied using the PP-PW method based on the density functional theory with *GGA*. The calculated equilibrium lattice parameters are in good agreement with the available experimental and theoretical data; validating the herein used method. A linear pressure dependence of the elastic stiffness's and bulk modulus were found. A set of isotropic parameters (bulk modulus, shear modulus, Young's

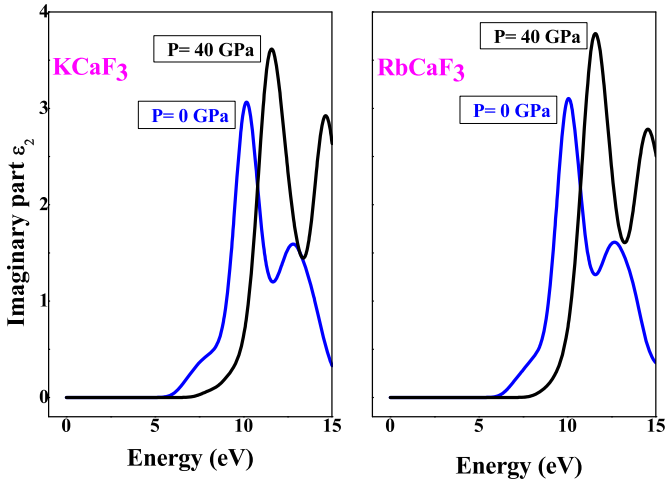

Fig. 7. The imaginary part as a function of photon energy for P = 0 and P = 40 GPa.

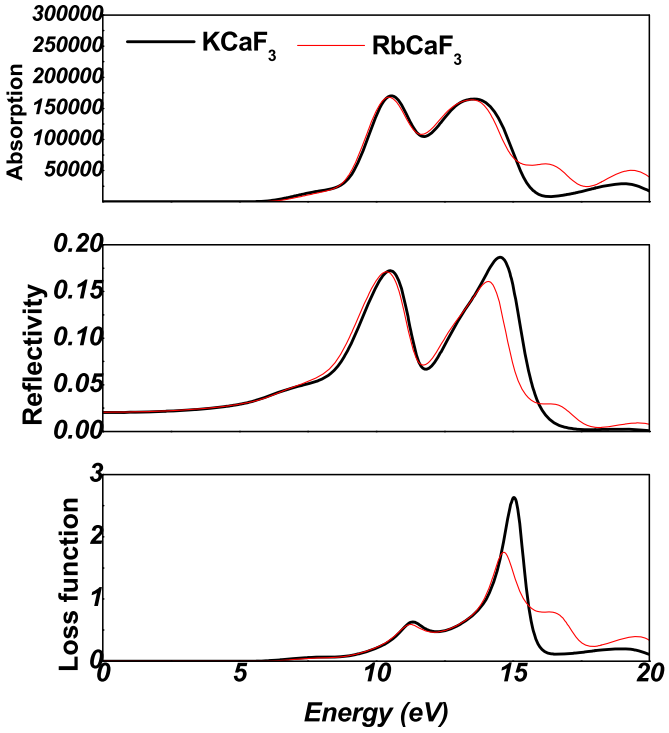

Fig. 8. The computed linear absorption, reflectivity and loss function.

modulus, Poisson's ration, average sound velocity and Debye temperature) are estimated for ideal polycrystalline $KCaF_3$ and $RbCaF_3$ aggregate. The calculated band structures show an insulating character of these materials with an indirect gap Γ–R at lower pressure and a direct gap Γ–Γ at high pressure. Analysis of the PDOS reveals that the upper valence band is essentially dominated by the F 2p with Ca-p and Ca-s states. The conduction band electron mobility and electrical conductivity of the herein studied materials are expected to be isotropic, while the valence band hole conductivity is expected to be anisotropic as well. The imaginary part of the dielectric function is calculated for radiation up to 15 eV. Using the band structure, we have analyzed the interband contribution to the optical response functions. The main peaks in the spectra correspond to the transition from the occupied state F_p (valence band) to the unoccupied states Ca: s or K, Rb: p (conduction band).

References

[1] Y.L. Liu, C.S. Shi, Mater. Res. Bull. 35 (2000) 689.
[2] G. Murtaza, Iftikhar Ahmad, A. Afaq, Solid State Sci. 16 (2013) 152.
[3] A.N. Belsky, P. Chevallier, E.N. Melchakov, C. Pedrini, P.A. Rodnyi, A.N. Vasilev, Chem. Phys. Lett. 278 (1997) 369.
[4] J. Tong, C. Lee, M.-H. Whangbo, R.K. Kremer, A. Simon, J. Köhler, Solid State Sci. 12 (2010) 680.
[5] F.A. Modine, E. Sonder, W.P. Unruh, Phys. Rev. B 10 (1974) 1623.
[6] D.Z. Demetriou, C.R.A. Catlow, A.V. Chadwick, G.J. Mclntyre, I. Abrahams, Solid State Ionics 176 (2005) 1571.
[7] G.W. watson, S.C. Parker, A. Wall, J. Phys. Condens. Matter 4 (1992) 2097.
[8] R.E. Boyett, M.G. Ford, P.A. Cox, Solid State Ion. 81 (1995) 61.
[9] B. Ghebouli, M.A. Ghebouli, M. Fatmi, A. Bouhemadou, Solid State Commun. 150 (2010) 1896.
[10] P. Goudochnikov, A.J. Bell, J. Phys. Condens. Matter 19 (2007) 176201.
[11] C. Li, B. Wang, R. Wang, H. Wang, X. Lu, Phys. B 403 (2008) 539.
[12] M.D. Segall, P.J.D. Lindan, M.J. Probert, C.J. Pickard, P.J. Hasnip, S.J. Clark, M.C. Payne, J. Phys. Condens. Matter 14 (2002) 2717.
[13] D. Vanderbilt, Phys. Rev. B 41 (1990) 7892.
[14] J.P. Perdew, K. Burke, M. Ernzerhof, Phys. Rev. Lett. 77 (1996) 3865.
[15] H.J. Monkhorst, J.D. Pack, Phys. Rev. B 13 (1976) 5188.
[16] B.G. Pfrommer, M. Côté, S.G. Louie, M.L. Cohen, Relaxation of crystals with the Quasi–Newton method, J. Comp. Phys. 131 (1997) 233.
[17] F. Birch, J. Geophys. Res. 83 (1978) 1257.
[18] R.E. Boyett, G. Ford, P.A. Cox, Solid State Ion. 81 (1995) 61.
[19] A. Bulou, C. Ridou, M. Rousseau, J. Nouet, A. Hewat, J. Phys. 41 (1980) 87.
[20] G.V. Sin'ko, N.A. Smirnov, J. Phys. Condens. Matter 14 (2002) 6989.
[21] J.F. Nye, Physical Properties of Crystals: Their Representation by Tensors and Matrices, Oxford University Press, Oxford, 1985.